ENVIRONMENT-INDUCED CRACKING OF MATERIALS

To order this title, and for more information, click here

Edited By
Sergei Shipilov, Metallurgical Consulting Services Limited, Toronto, Canada
Russell Jones, Exponent Failure Analysis Associates, U.S.A.
Jean-Marc Olive, University of Bordeaux 1, France
Raúl Rebak, Lawrence Livermore National Laboratory, U.S.A.

Description

Environmental assisted cracking of metals is an important topic related to many industries in lives. Although the problem with this type of corrosion has been known for many years, the debate on the effects and possible remedies available under different environmental conditions is ongoing and topical. Previous volumes have tended to concentrate on single aspects and causes (e.g. stress corrosion fracture), while ignoring other mechnisms such as hydrogen embrittlement, corrosion fatigue and more modern concerns such as the near neutral SCC pipelines).

Audience

Conference attendees, university libraries, research and testing laboratories, companies specialising in corrosion control and prevention, and other corrosion experts and consultants

Contents

stainless steel (M. Menard, J.M. Olive, A.-M. Brass and I. Aubert) 14. Hydrogen effects on the plasticity of nickel and binary nickel-chromium alloy (D. Delafosse, G. Girardin and X. Feaugeas) 15. Hydrogen-assisted cracking of iron-based amorphus alloys: experimental and finite element observations (N. Eliaz, L. Banks-Sills, D. Ashkenazi and R. Eliasi)

Section 3. Hydrogen Permeation and Transport
16. Quantification of hydrogen transport and trapping in ferritic steels with the electrochemical permeation technique (A.-M. Brass) 17. Hydrogen diffusivity and straining effect at cathodic polarization of A1 in NaOH solution (E. Lunarska and O. Chernyayeva) 18. Visualization of hydrogen diffusion path by a high sensitivity hydrogen microprint technique (S. Matsuda, K. Ichitani and M. Kanno) 19. Effect of deformation type on the hydrogen behavior in high-strength low-alloy steel (E. Lunarska and K. Nikiforow) 20. Strain-assisted transport of hydrogen and related effects on the intergranular stress corrosion cracking of alloy 600 (J. Chene) 21. Hydrogen in trapping states harmful and resistant to environmental degradation of high-strength steels (K. Takai)

Section 4. Hydrogen-Assisted Cracking and Embrittlement
22. Ductile crack initiation and growth promoted by hydrogen in steel (Y. Shimomura and M. Nagumo) 23. Hydrogen assisted stress-cracking behaviour of supermartensitic stainless steel weldments (W. Dietzel, P. Bala Srinivasan and S.W. Sharkawy) 24. Hydrogen-assisted fracture of inertia welds in 21Cr-6Ni-9Mn stainless steel (B.P. Somerday, S.X. McFadden, D.K. Balch, J.D. Puskar and C.H. Cadden) 25. Embrittlement of metals in a hydrogen medium (N.M. Vlasov and I.I. Fedik)

Section 5. Nonferrous Alloys
26. Stress corrosion cracking of magnesium alloy with the slow strain-rate technique (H. Uchida, M. Yamashita, S. Hanaki and T. Nozaki) 27. Measurement and modeling of crack conditions during the environment-assisted cracking of an Al-Zn-Mg-Cu alloy (K.R. Cooper and R.G. Kelly) 28. Influence of composite materials on the stress corrosion cracking of aluminium alloys (F. Lu, W. Chang, G. Zhu, X. Zhang and Z. Tang) 29. Study on stress corrosion cracking of aluminium alloys in marine atmosphere (X. Zhang, Z. Sun, Z. Tang, M. Liu and B. Li) 30. Potential-pH map for environment-assisted cracking of Ti-6Al-4V (T. Haruna, M. Hamasaki and T. Shibata) 31. On the competitive effects of water vapor and oxygen on fatigue crack propagation at 550ºC in a Ti6242 alloy (C. Sarrazin-Baudoux, F. Loubat and S. Potiron) 32. Effect of supercritical water on fatigue crack propagation in a titanium alloy (F. Loubat and J.M. Olive) 33. Microstructural sensitivity of stress corrosion cracking in copper alloys due to dynamic recrystallization (L. Lin, Y. Zhao, D. Cui and Y. Meng)

Section 6. Iron and Nickel Based Alloys
34. Susceptibility to and the mechanism of stress corrosion cracking in structural alloys in aqueous solutions (A.N. Kumar) 35. Corrosion-fatigue properties of surface-treated surgical implant stainless steel X2CrNiMo18-15-3 (G. Mori, H. Wieser and H. Zitter) 36. Stress corrosion cracking of austenitic stainless steel Type 316 in acid solutions and intergranular SCC mechanism: effects of anion species (Cl^- and SO_4^{2-}) and sensitizing temperature (R. Nishimura, A.

Sulaiman and Y. Maeda) 37. Environmentally assisted cracking of nickel alloys - a review (R.B. Rebak)

Section 7. Ceramics and Glasses
38. Environment induced crack growth of ceramics and glasses (R.H. Jones) 39. Study of delayed fracture of PZT-5 ferroelectric ceramics (K.W. Gao, Y. Wang, L.J. Qiao and W.Y. Chu)

Section 8. Liquid Metal Embrittlement
40. Liquid metal-induced embrittlement of a Fe9Cr1Mo martensitic steel (J.-B. Vogt, I. Serre, A. Verleene and A. Legris) 41. Liquid metal embrittlement by lead of high chromium martensitic steel bolts (K. Nakajima, S. Inagaki, T. Taguchi, M. Arimura and O. Watanabe) 42. Liquid metal embrittlement of superplastic alloys (A.I. Malkin, Z.M.

and V.P. Kholodenko)

Section 6. Degradation of Materials Under In-Service Conditions
23. Stress corrosion cracking of carbon steel in fuel ethanol service (J. G. Maldonado and R.D. Kane) 24. Hydrogen degradation of steels under long-term in-service conditions (H.M. Nykyforchyn, K.-J. Kurzydlowski and E. Lunarska) 25. Corrosion and hydrogen absorption of commercial reinforcing steel in concrete after 33 years of service on the Baltic Sea beach (S.M. Beloglazov, K.V. Egorova and N.V. Kolesnikova) 26. Stress corrosion cracking of aluminium brass induced by marine organism fouling (L. Lin and Y. Zhao) 27. Modeling of prior exfoliation corrosion in aircraft wing skins (M. Liao, G. Renaud, D. Backman, D.S. Forsyth and N.C. Bellinger)

Section 7. Stress Corrosion Cracking Case Studies
28. Case studies of corrosion and environmentally induced cracking in industry (I. Le May and C. Bagnall) 29. Stress corrosion cracking: cases in refinery equipment (G.R. Lobley) 30. Embrittlement cracking of a stabilized stainless steel wire mesh in an ammonia converter (V. Kain, V. Gupta and P.K. De) 31. Environment-induced transgranular stress corrosion cracking of 304L stainless steel instrument line tubes (M. Clark, O. Yong, A.M. Brennenstuhl and M. Lau) 32. Stress corrosion cracking of austenitic stainless steel in a nuclear power plant environment (M. Brezine and L. Kupca)

Section 8. New Test Methods for SCC Studies
33. High-resolution, in-situ, tomographic observations of stress corrosion cracking (T.J. Marrow, L. Babout, B.J. Connolly, D. Engelberg, G. Johnson, J.-Y. Buffiere, P.J. Withers and R.C. Newman) 34. Detection of SCC by the simultaneous use of electrochemical noise and acoustic emission measurements (M. Leban, Z. Bajt, J. Kovac and A. Legat) 35. Circumferential notch tensile (CNT) tests for determination of K_{ISCC}, using small fracture mechanics specimens (R. Rihan, R.K. Singh Raman and R.N. Ibrahim) 36. Development of spiral notch torsion test: a new fracture mechanics approach to determination of K_{ISCC} (R.K. Singh Raman, R. Bayles, S.P. Knight, Jy-An Wang, B.R.W. Hinton and B.C. Muddle) 37. Issues in stress corrosion testing of welded super martensitic stainless steels for oil and gas pipelines (A. Turnbull and B. Nimmo) 38. Evaluation of the resistance to hydrogen embrittlement by the slow bending test (M. Cabrini, G.D'Urso and T. Pastore) Author Index Subject Index

Bibliographic & ordering Information
Hardbound, 1000 pages, publication date: NOV-2007
ISBN-13: 978-0-08-044635-6
ISBN-10: 0-08-044635-3
Imprint: ELSEVIER
Price: Order form
GBP 150
USD 265
EUR 220

Books and book related electronic products are priced in US dollars (USD), euro (EUR), and Great Britain Pounds (GBP). USD prices apply to the Americas and Asia Pacific. EUR prices apply in Europe and the Middle East. GBP prices apply to the UK and all other countries.

See also information about conditions of sale & ordering procedures, and links to our regional sales offices.

060/651
Last update: 11 Dec 2007

Printer-friendly version

Environment-Induced Cracking of Materials

Volume 1: Chemistry, Mechanics and Mechanisms

Proceedings of the Second International Conference on Environment-Induced Cracking of Metals (EICM-2), The Banff Centre, Banff, Alberta, Canada, September 19–23, 2004

Edited by

S.A. Shipilov
Metallurgical Consulting Services, Calgary, Alta., Canada

R.H. Jones
Exponent Failure Analysis Associates, Bellevue, WA, USA

J.-M. Olive
Université Bordeaux 1, Talence Cedex, France

R.B. Rebak
Lawrence Livermore National Laboratory, Livermore, CA, USA

Contents

Section 2 CRACK GROWTH MECHANISMS

Section 3 HYDROGEN PERMEATION AND TRANSPORT

Section 4 HYDROGEN-ASSISTED CRACKING AND EMBRITTLEMENT

Section 5 NONFERROUS ALLOYS

Section 6 IRON AND NICKEL BASED ALLOYS

Section 7 CERAMICS AND GLASSES

Section 8 LIQUID METAL EMBRITTLEMENT

Section 9 HISTORY OF SCC RESEARCH

Environment-Induced Cracking of Materials

Volume 2:
Prediction, Industrial Developments and Evaluation

Proceedings of the Second International Conference on Environment-Induced Cracking of Metals (EICM-2), The Banff Centre, Banff, Alberta, Canada, September 19–23, 2004

Edited by

S.A. Shipilov
Metallurgical Consulting Services, Calgary, Alta., Canada

R.H. Jones
Exponent Failure Analysis Associates, Bellevue, WA, USA

J.-M. Olive
Université Bordeaux 1, Talence Cedex, France

R.B. Rebak
Lawrence Livermore National Laboratory, Livermore, CA, USA

Contents

Modelling of primary water stress corrosion cracking (PWSCC) at control rod drive mechanism (CRDM) nozzles of pressurized water reactors (PWR)

O.F. Aly [a], A.H.P. Andrade [a], M. Mattar Neto [a], M. Szajnbok [b], H.J. Toth [a]

[a] *IPEN-Energy and Nuclear Research Institute, Av. Lineu Prestes 2.242, 05508-900 São Paulo, SP, Brasil*

[b] *EPUSP-Polytechnic School of São Paulo University, Av. Lineu Prestes 580, 05508-900 São Paulo, SP, Brasil*

Abstract

One of the main causes of failure in pressurized water reactors (PWR) is the stress corrosion cracking (SCC) at control rods drive mechanism (CRDM) nozzles, produced by tensile stress, temperature, susceptible metallurgical microstructure and environmental conditions of the primary water. Such cracks can cause accidents that reduce nuclear safety by blocking the rods displacement at CRDM and/or leakage of primary water. This paper will present a preliminary development of a model to predict such damage, including initiation and propagation of primary water SCC (PWSCC). The model assumes the Pourbaix potential-pH diagram for Alloy 600 on the typical PWR environment, primary water at high temperature. Over this diagram, the region where the SCC submodes can occur is plotted. Submodes are determined by regions of potential where various modes of surface material-environment interactions can occur, such as stress corrosion, pitting, generalized corrosion or passivation. Over these regions an empirical-probabilistic is linked to a strain rate damage model that can evaluate the time to failure and the damage parameter, as a function of total stress at the material surface, its temperature and other factors depending on environment-material combination and thermomechanical treatment of this alloy.

1. Introduction

Degradation of materials during operation – mainly corrosion, fatigue and irradiation – represents one of the main technological factors that may limit the reliability and safety of nuclear power plants [1]. One of the modes that causes risks to pressurized water reactors (PWRs) is the stress corrosion cracking (SCC) of steels and alloys. The cracks (axial or circumferential) may cause accidents such as leaking of coolant [2], nozzle components ejection and blocking of the rod drive mechanism at

CRDM (control rods drive mechanism) [3]. Leakage of coolant/primary water can cause general corrosion in the low-alloy vessel head by boron deposits.

Most Western PWRs have CRDM penetration in the pressure vessel head made of stainless steel and Alloy 600. The composition of Alloy 600 is primarily >72% Ni, 14–17% Cr, 6–10% Fe [3–5]. The yield strength of the alloy varies from 213 to 517 MPa. Normally this alloy is mill annealed at 885°C, and final annealed for 4–6 h followed by air cooling. Nevertheless such a treatment can be varied depending on its purpose. The Alloy 600 works with some variation at 315°C and 15.5 MPa in pure water [3].

The primary water SCC (PWSCC) appears in the lower part of each nozzle that is fabricated in Alloy 600 and welded to the internal vessel head surface with dissimilar material such as Alloy 182. There are typically 40–90 penetrations per vessel that may include some spare penetrations which are not fitted with CRDM or through core instrumentation of PWR [6].

2. Models and modelling

SCC nucleation and propagation are very complex phenomena. SCC is one modality of environment-assisted cracking (EAC) besides corrosion fatigue and hydrogen embrittlement, depending on several variables that can be classified in microstructural, mechanical, and environmental terms [7,8]. Microstructural variables are: (i) grain boundary microchemistry and segregation, M; (ii) thermal treatment, TT, that can cause intragranular and intergranular metallic carbide distribution; and (iii) grain size, gs, and cold work, CW, or plastic deformation. The second two variables fix another variable such as the yield stress, s_{YS}. Mechanical variables are: (i) residual stress, s_r; (ii) applied stress, s_a (a tension stress and geometry can be summarized as a stress intensity factor, K_I); and (iii) strain e and strain rate $\dot{e}$. Environmental variables include: (i) temperature, T; (ii) $[H]^+$ or pH; (iii) solution or water chemistry, SC; (iv) inhibitors or pollutants in solution; (v) electrochemical potential, V; and (vi) partial pressure of hydrogen, p_{H2} [9]. Environmental cracking susceptibility can be expressed as [10]:

$$SCC = f(M, TT, gs, CW, K_I, e, \dot{e}, T, pH, SC, V, p_{H2}) \quad (1)$$

Fig. 1 summarizes the main processes by which the above conditions at grain boundaries lead to SCC [11].

There are several models to express these phenomena mathematically: (i) the slip dissolution/film rupture by Ford and Andresen [13]; (ii) the enhanced surface mobility theory by Galvele [14]; (iii) coupled environment fracture model by Macdonald and Urquidi-Macdonald [15]; (iv) the internal oxidation mechanism by Scott and Le Calvar [16]; (v) numerical model by Rebak and Smialowska [17] and by Seung-gi and Il Soon Hwang [18]; and (vi) hydrogen-induced cracking models by Shen and Shewmon, and Magnin et al. (see Ref. [10]). For a comprehensive review of several of these models, see Ref. [10], and for hydrogen action models see Refs. [19,20]. Two kinetic models, including an empirical-probabilistic model and a deterministic strain rate damage model [21], were chosen to develop the model presented in this work.

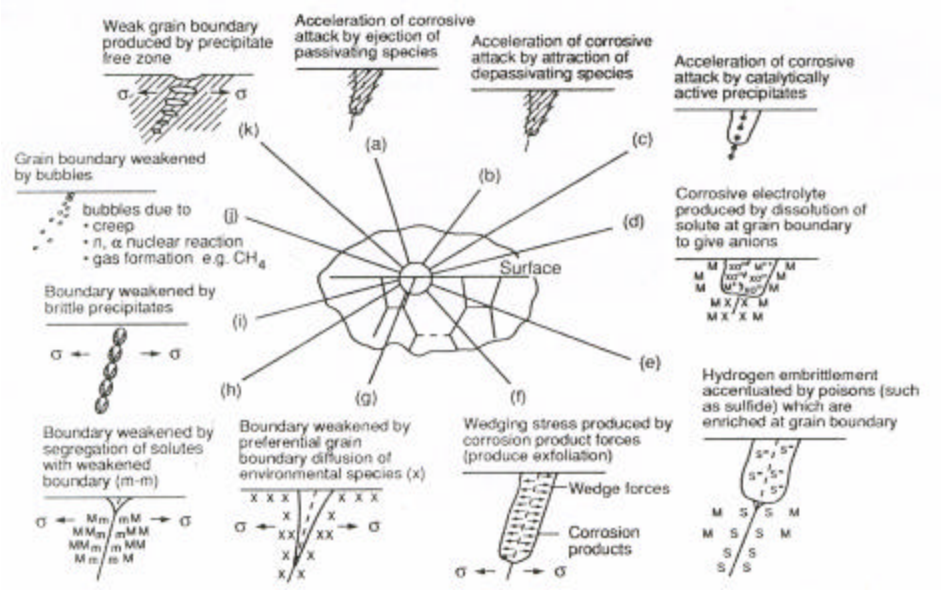

Fig. 1. The processes starting from (a) to (k) range from the mostly chemical to the mostly mechanical [11].

The empirical-probabilistic model is derived from the general dependencies of time-to-failure shown in Eq. (2) treated statistically:

$$t_f = d[H^+]^{-m}\sigma^{-n}\exp\left(\frac{Q}{RT}\right) \tag{2}$$

where t_f = time to failure, s = stress, n = exponent of stress, Q = thermal activation energy, T = absolute temperature (K), R = gas constant, $[H^+]$ = hydrogen ion activity, m = exponent of hydrogen ion activity, and d = constant [11].

The model proposed in Ref. [22] is a simplification of Eq. (2) that can be converted into a form more convenient to use as:

$$t_f = A\, t_{ref}\left(\frac{\sigma}{\sigma_{ref}}\right)^n \exp\left[\left(\frac{Q}{R}\right)\left(\frac{1}{T}-\frac{1}{T_{ref}}\right)\right] \tag{3}$$

where A = non-dimensional material constant reflecting the effect of material properties on time to 1% PWSCC, t_{ref} = time to selected fraction of PWSCC for a reference case, s_{ref} = reference value of stress, and T_{ref} = reference value of temperature.

The 2-parameter Weibull statistical distribution describes the variation of PWSCC as time function as:

$$F = 1 - \exp\left[-\left(\frac{t}{\theta}\right)^{b}\right] \tag{4}$$

where F = fraction of population of components under consideration all susceptible to the same failure mode that experience PWSCC, t = time normally given in effective full power years (EFPY), b = Weibull slope, a fitted parameter determined by analysis of failure data, and q = Weibull characteristic time that corresponds to the time when 63.2% of the components have experienced PWSCC. This parameter can be written as $t_f = t_{1\%}$:

$$q = \frac{t_{1\%}}{(0.0101)^{1/b}} \tag{5}$$

Eqs. (4) and (5) combined yield Eq. (6):

$$F = 1 - \exp\left[-0.0101\left(\frac{t}{t_{1\%}}\right)^{b}\right] \tag{6}$$

The value of $t_{1\%}$ together with an appropriate value for the Weibull slope, b, determine the complete prediction for PWSSC as a time function using Eq. (6). More detail on this model, plus several examples that were solved, are given in Refs. [11,22].

The strain rate damage model is essentially a semi-empirical model theory of SCC, where strain rate rather than stress is considered to be the main mechanical variable. The main parameter of this model is the damage parameter, D, that includes the initiation and propagation stages of the cracks. It begins essentially from a semi-empirical theory of SCC, based on the analogy with Tresca criterion to plastic flow. It formalized the strain rate as a moving factor in a damage model that allows quantitative predictions on serviceable life which in turn depends on SCC. A damage function is defined as a mode linked to a component submitted to a strain rate history. When this damage function reaches a critical value, it can predict the SCC. The critical value of this damage function depends on the material in question and environment

$$D = \int_0^t A\,[\dot{e}\,(t)]^p\,dt, \qquad [D] = [\text{length}] \tag{7}$$

where t = time, $\dot{e}\,(t)$ = total strain rate, A and p = parameters that depend on material-environment combination.

In Eq. (7), the strain is divided into elastic and a non-elastic:

$$\dot{e}\,(t) = \dot{e} = \dot{e}_e + \dot{e}_n \tag{8}$$

It is then necessary to adjust the experimental true stress-true strain data in accordance with Eq. (8). This can be accomplished using the Bodner-Partom constitutive equation that assumes Eq. (8) where the applied uniaxial stress s is related to the non-elastic strain rate $\dot{e}_n$ by

$$\dot{e}_n = \frac{2D_0}{\sqrt{3}} \exp\left[-\frac{1}{2}\left(\frac{Z}{s} \right)^{2n} \right] \tag{9}$$

where D_0 is a constant, n is a temperature-dependent material parameter, and Z is a function related to strain hardness. When thermal recovery is neglected, the hardness function Z is such that

$$Z = Z_1 - (Z_1 - Z_0)\exp(-mW_p) \tag{10}$$

where the inelastic strain energy density is

$$W_p = \int s \, d\, \dot{e}_n \tag{11}$$

The temperature-dependent constants in the above equations might be written as:

$$\mathrm{n} = \frac{\mathrm{a}}{\mathrm{T}} + \mathrm{b} \tag{12}$$

$$m = m_0 T + c_0 \tag{13}$$

$$Z_0 = Z_1(m_1 T + c_1) \tag{14}$$

Hence the list of material constants in Bodner-Partom's model include D_0, a, b, Z_1, m_1, c_1, m_0, and c_0.

Thus, the model needs at least three values of stress and strain at two different strain rates at each of two temperatures as the minimum data set to determine these constants. In brief, in this model, we have formalized the concept of strain rate as a driving force in a damage model that permits quantitative predictions of stress corrosion lifetimes through a damage function defined as dependent on the strain rate history of a component. SCC is predicted when this damage function reaches a critical value. The critical damage value depends on both the material in question and the environmental condition of interest. The principal advantage of this model is that it's not necessary to distinguish between cracking initiation and propagation [21,22]. More detail on this model, plus modelling examples, are given in Ref. [22].

3. Proposed model

Staehle [11] has proposed a 3-dimensional diagram in accordance with Fig. 68 of Ref. [11]. It shows the thermodynamic conditions to occur at the modes of PWSCC in Alloy 600. The base is the 2-dimensional potential-pH (known as Pourbaix) diagram for this material in primary water at high temperature (300 to 350 °C) (Fig. 2). It superimposes the corrosion submodes based on experimental data from the literature. Submodes are determined by regions of potential where the different modes of surface material-environment interactions can occur, such as SCC, pitting, generalized corrosion, and passivation. The third dimension is the "useful strength" of the material as affected by the environment at that point, the strength fraction. Staehle [11]

explained that the third variable could be a crack velocity for the vertical coordinate, instead of the strength fraction, because the data are sparse and the component experiments with reference to this diagram used different methods of loading states and data analysis.

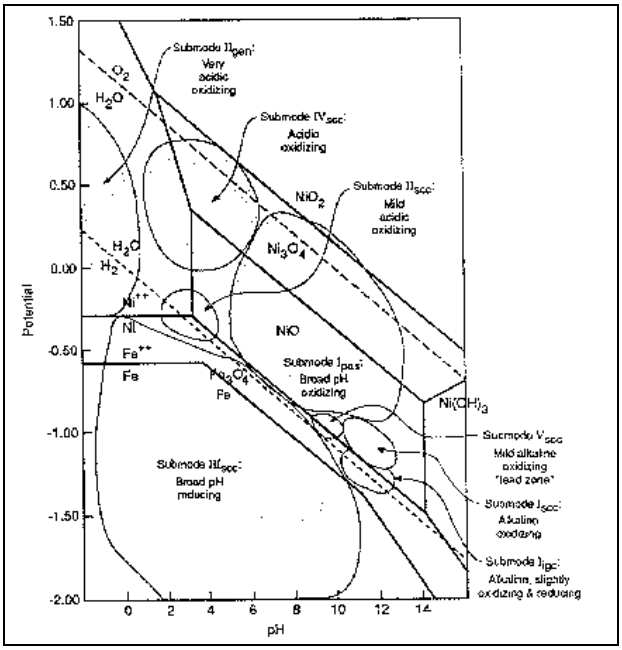

Fig. 2. Pourbaix diagram for Alloy 600 at ~300°C used as a base for submode regions of the 3-dimensional (*V*-pH-strength fraction) diagram (Fig. 68 from Ref. [11]).

It is proposed that the model be framed over the same Pourbaix (*V*-pH) diagram for Alloy 600 in the typical environment, namely water at high temperature. Over this diagram is plotted the region where the SCC submodes can occur. Firstly, over one of these regions will be coupled a strain rate damage model that can describe the damage parameter evolution with time and an empirical-probabilistic one that can describe the time to failure, normally expressed in terms of EFPY as a function of a total stress at the material surface, its temperature and parameters depending on environment-material combination and thermomechanical treatment of the alloy. Then, we will test the model using data from the literature plus data obtained using the new slow strain rate tensile (SSRT) test equipment installed at CDTN in Brazil [12]. Thus, this model could be used for a Brazilian nuclear power plant taking into consideration the plant materials and the characteristics of its design and operation, including the heat material fabrication processes, material composition, plant thermomechanic history, primary water chemical composition, and operational temperature conditions at this plant.

4. Preliminary results

A computer worksheet was created to plot an empirical-probabilistic model to be fed with data. This is represented by Eqs. (3)–(6), as was done in Refs. [11,22]. Fig. 3 was created using data of Table 1 from Ref. [23] with *b*-Weibull slope parameter equal to 1.5 to check the reproduction of the model.

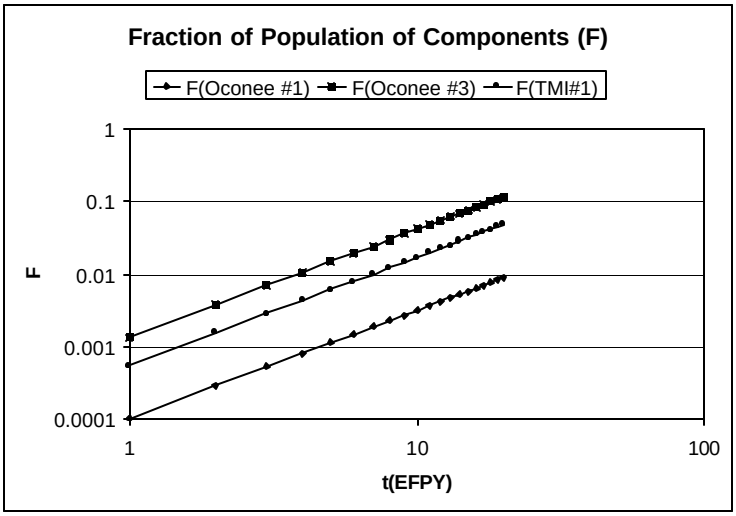

Fig. 3. Diagram showing plotted curves for three nuclear plants referred in Table 1 of Ref. [23].

If it is known how long a plant has operated in the submode III_{SCC} (see Fig. 2), this length of time can be used to couple the curves of Fig. 3 with Pourbaix diagram and thus to estimate a parameter *F* by Eq. (4) that represents the fraction of population of all components susceptible to the same degradation submode that experiences PWSCC.

5. Analysis and discussion

The above empirical model serves as a highly practical method for the prediction of PWSCC. Using Eqs. (2) and (6), a higher *F* is expected for the lower pH. It is necessary to relate a damage initiation with the variations of pH and *V* in the PWSCC domain. These values are usually below an equilibrium borderline for Ni/NiO [16,19]. It is therefore necessary to verify the suppositions through empirical tests. Referring to the plants considered in Fig. 3, it is desirable to know which pH and *V* values should be employed for each of them to operate efficiently.

The crack growth rate presents a dependence with pH shown in Eq. (15) from Ref. [25]:

$$\frac{dD}{dt} = CGR = C\left(\frac{pH}{7.5}\right)^2 \qquad \text{for } 7.5 = \text{pH} = 9 \tag{15}$$

If it is considered that the crack initiation and growth combined to constitute damage, it is possible that the crack initiation can follow the same law-time integrated with differently adjusted parameters (constant *C*), for initiation and growth. Clearly this must be investigated. In both models, it is necessary to obtain the relationship between the time to failure and the variation in *V* and pH in PWSCC domain through experimental tests using SSRT technique in CDTN.

The strain rate damage model has the advantage of describing the evolution of damage with time, while the empirical probabilistic model has the advantage of being more simple to apply. The strain rate damage model reduces to empirical model when one of the suggested models for creep behaviour of Alloy 600 is used in its formulation [22] according to Ref. [24].

6. Conclusions

This paper presents a preliminary development of a combined model composed of the Pourbaix (potential-pH) diagram linked with a kinetic model as well as with empirical probabilistic and deterministic strain rate damage models. The use of the Pourbaix diagram has the advantage of revealing the thermodynamic conditions required to initiate SCC. The use of the kinetic empirical-probabilistic model linked with Pourbaix diagram has the advantage of obtaining the statistical estimation of the time to failure. The use of the kinetic strain rate damage model has the advantage of obtaining the deterministic strain rate damage parameter evolution with time. Data from the Brazilian CDTN will be used to validate the model proposed in this study.

References

[1] J.T.A. Roberts, Structural Materials in Nuclear Power Systems, Plenum Press, New York, 1981.

[2] V.N. Shah, A.G. Ware, A.M. Porter, Assessment of pressurized water reactor control rod drive mechanism nozzle cracking, Idaho National Engineering Laboratory, NUREG/CR-6245, Idaho Falls, October 1994.

[3] J. Medoff, Primary water stress corrosion cracking of vessel head penetration nozzles, Presented for the USNRC CEOG Executive Meeting Report, May 2001.

[4] ASME, Boiler and Pressure Vessel Code, Section II, Materials Specifications, Part A, Ferrous Materials, ASME, Philadelphia, 1998.

[5] M.A. Rinckel, Nucl. Eng. Des. 181 (1998) 17–39.

[6] IAEA, Assessment and Management of Ageing of Major Nuclear Power Plant Components Important to Safety: Pressurized Water Reactor Pressure Vessels, IAEA-TECH DOC, Vienna, 1997.

[7] M.G. Fontana, N.D. Greene, Corrosion Engineering, McGraw-Hill, New York, 1978.

[8] R.W. Hertzberg, Deformation and Fracture Mechanics of Engineering Materials, John Wiley & Sons, New York, 1989.

[9] N. Totsuka, Z. Szklarska-Smialowska, Hydrogen induced IGSCC of Ni-containing FCC alloys in high temperature water, in: G.J. Theus, J.R. Weeks (Eds.), Proc. 3rd International Symposium on Environmental Degradation of Materials in Nuclear Power Systems–Water Reactors, TMS, Warrendale, 1987, pp. 691–696.

[10] R.B. Rebak, Z. Szklarska-Smialowska, Corros. Sci. 38 (1996) 971–988.
[11] R.W. Staehle, Combining design and corrosion for predicting life, in: R.N. Parkins (Ed.), Life Prediction of Corrodible Structures, vol. 1, NACE International, Houston, 1994, pp. 138–291.
[12] P.A.P. Moreira, A.H.P. Andrade, M.M.A.M. Schvartzman, C.F.C. Neves, Testing facility for stress corrosion cracking material characterization in PWR operational environment, in: Proc. 57th Annual Congress of ABM (Associação Brasileira de Metalurgia e Materiais), held July 2002, São Paulo, Brazil, pp. 1144–1154 (in Portuguese).
[13] P.L. Andresen, F.P. Ford, Mater. Sci. Eng. A103 (1988) 167–184.
[14] J.R. Galvele, Corros. Sci. 27 (1987) 1–33.
[15] D.D. Macdonald, M. Urquidi-Macdonald, Modelling of the electrochemistry of stress corrosion cracks in sensitized Type 304SS in boiler water reactors, in: D. Cubicciotti (Ed.), Proc. 4th International Symposium on Environmental Degradation of Materials in Nuclear Power Systems–Water-Reactors, NACE, Houston, 1990, pp. 4-1–4-11.
[16] P.M. Scott, M. Le Calvar, Some possible mechanisms of intergranular stress corrosion cracking of Alloy 600 in PWR primary water, in: R.E. Gold, E.P. Simonen (Eds.), Proc. 6th International Symposium on Environmental Degradation of Materials in Nuclear Power Systems–Water Reactors, TMS, Warrendale, PA, 1993 pp. 657-665.
[17] R.B. Rebak, Z. Szklarska-Smialowska , Mechanism of stress corrosion cracking of Alloy 600 in high temperature water, in: G. Airey et al. (Eds.), Proc. 7th International Symposium on Environmental Degradation of Materials in Nuclear Power Systems–Water Reactors, NACE, Houston, 1995, pp. 855–865.
[18] S.-G. Lee, I.S. Hwang, Probabilistic prediction model for initiation time on Alloy 600 CRDM nozzle, in: Proc. Korean Nuclear Society Autumn Meeting, KNS, Seoul, 1999.
[19] F. Foct, Stress corrosion mechanisms in monocrystalline and polycrystalline alloy 600 on PWR: hydrogen effects, Ph.D. Thesis, Grenoble, 1999 (in French).
[20] D. Caron, Hydrogen influence on the stress corrosion cracking on Alloy 600 in the primary water of pressurized water reactors, Ph.D. Thesis, Lyon, 2001 (in French).
[21] J.A. Begley, Strain-rate Damage Model for Alloy 600 in Primary Water, EPRI Report NP-7008, EPRI, Pittsburg, 1990.
[22] J.A. Gorman, K.D. Stavropoulos, W.S. Zemitis, M.E. Dudley, PWSCC Prediction Guidelines, EPRI Final Report TR-104030 Project 2812-15, July 1994.
[23] USNRC, Preliminary Staff Technical Assessment for Pressurized Water Reactor Vessel Head Penetration Nozzles Associated with NRC Bulletin 2001-1, Circumferential Cracking of Reactor Pressure Vessel Head Penetration Nozzles, November 2001.
[24] O. Leclercq, F. Vaillant, Creep Behavior Study at 350°C of Alloy 600, Report HT 40/NTE 1140-A, Eletricité de France, February 1991 (in French).
[25] EPRI, Crack Growth Rates for Evaluating Primary Water Stress Corrosion Cracking (PWSCC) of Thick-Wall Alloy 600 Material, MRP-55, 2002.